KJO
pISSN: 1011-8942 eISSN: 2092-9382

Korean J Ophthalmol 2022;36(6):518-526
https://doi.org/10.3341/kjo.2022.0089

Original Article

Fractal Dimension of Peripapillary Vasculature in Primary Open-Angle Glaucoma

Chae Hyun Song[1], Seok Hwan Kim[2], Kyoung Min Lee[2]

[1]*Department of Ophthalmology, Seoul National University Hospital, Seoul National University College of Medicine, Seoul, Korea*
[2]*Department of Ophthalmology, Seoul Metropolitan Government Seoul National University Boramae Medical Center, Seoul National University College of Medicine, Seoul, Korea*

Purpose: To compare the fractal dimensions of the peripapillary microvasculature as obtained by optical coherence tomography angiography (OCTA) between primary open-angle glaucoma (POAG) and controls.

Methods: Optic nerve head and peripapillary area images were taken using the 20° × 20°-scan of Spectralis OCTA (Heidelberg Engineering) in 97 subjects (64 POAG patients, 33 control patients). The optic nerve head microvasculature was evaluated according to predefined slabs: the superficial vascular complex (SVC) and the avascular complex (AVC). The *en face* image of each slab was processed by ImageJ software (National Institutes of Health) in order to calculate the vessel density and the fractal dimension using the box-counting method. For comparison, the peripapillary retinal nerve fiber layer (RNFL) thickness was obtained from Spectralis OCT circle scans. The utilities of the parameters for discriminating between the POAG and control groups were assessed using areas under the receiver operating characteristic curves (AUCs).

Results: The SVC fractal dimension was lower in the POAG than in the control group ($p < 0.001$), while AVC showed no intergroup difference ($p = 0.563$). The fractal dimension showed a good correlation with the vessel density in both SVC and AVC (both $p < 0.001$). In a multivariable regression analysis, the SVC fractal dimension was negatively correlated with age ($p < 0.001$) and axial length ($p < 0.001$) and positively correlated with average RNFL thickness ($p < 0.001$), while the AVC fractal dimension was positively correlated with the Bruch's membrane opening size ($p = 0.013$). In terms of diagnostic utility, the AUC was significantly larger for the average RNFL thickness (AUC, 0.889) than for the SVC fractal dimension (AUC, 0.772; $p = 0.008$).

Conclusions: The fractal dimension of SVC was associated with the average RNFL thickness and was reduced in POAG patients. Fractal dimension analysis could be used in evaluating peripapillary vascularity by OCTA.

Key Words: Fractal dimension, Optical coherence tomography angiography, Peripapillary microvasculature, Primary open-angle glaucoma

Received: July 6, 2022 *Final revision:* August 24, 2022
Accepted: September 26, 2022

Corresponding Author: Kyoung Min Lee, MD. Department of Ophthalmology, Seoul Metropolitan Government Seoul National University Boramae Medical Center, Seoul National University College of Medicine, 20 Boramae-ro 5-gil, Dongjak-gu, Seoul 07061, Korea. Tel: 82-02-870-2413, Fax: 82-02-831-0714, E-mail: isletzz@gmail.com

The peripapillary microvasculature is a subject of great interest with regard to optic nerve head (ONH) evaluation for glaucoma assessment. Glaucoma patients suffer reduced peripapillary retinal blood flow [1,2], which can be interpreted either as an etiologic factor [3-5] or the consequence of diminished metabolic demand due to glaucoma-

© 2022 The Korean Ophthalmological Society
This is an Open Access journal distributed under the terms of the Creative Commons Attribution Non-Commercial License (http://creativecommons.org/licenses/by-nc/4.0/) which permits unrestricted non-commercial use, distribution, and reproduction in any medium, provided the original work is properly cited.

tous optic neuropathy [1,2,6,7]. With the advent of optical coherence tomography angiography (OCTA), the peripapillary microvasculature could be visualized noninvasively without dye injection, which advance has prompted many studies in which primary open-angle glaucoma (POAG) patients are consistently reported to have reduced peripapillary microvasculature density [8-11].

Vascular density findings, however, are affected by image scale and resolution. And, due to the detection limit of a vessel size, a microvasculature smaller than the limit would be overlooked when calculating vascular density. This problem can be handled by the use of fractal analysis. Fractal analysis fills the overlooked area with multiple levels of subunits that resemble the structure of the entire object. The fractal dimension, as a noninteger between 1 and 2, describes the lacunarity of space: that is, it shows how densely a space is filled without being affected by the scale and resolution limit. Fractal analysis and the fractal dimension have been used for evaluation of retinal vasculature in many studies [12-21]. To the best of our knowledge, however, there has been no evaluation of OCTA based peripapillary microvasculature using fractal dimension analysis. The purpose of this study, then, was to compare the fractal dimension of the peripapillary microvasculature between POAG and control eyes in order to present a novel ONH parameter representing peripapillary vascularity.

Materials and Methods

Ethics statement

The study protocol was approved by the Institutional Review Board of Seoul Metropolitan Government Seoul National University Boramae Medical Center and adhered to the tenets of the Declaration of Helsinki. Written informed consent to participate was obtained from all of the subjects.

Study design

This investigation included subjects who had been enrolled in the Boramae Glaucoma Imaging Study (BGIS), an ongoing prospective study at the Seoul Metropolitan Government Seoul National University Boramae Medical Center. It registered the anatomic features of the ONH in subjects who had visited our institution with either a diagnosis of glaucoma or suspicion of glaucoma.

Subjects who had been enrolled in the BGIS underwent comprehensive ophthalmologic examinations that included best-corrected visual acuity assessment, refraction, slit-lamp biomicroscopy, Goldmann applanation tonometry, gonioscopy, dilated funduscopic examination, keratometry (RKT-7700; Nidek, Hiroshi, Japan), axial length measurement (IOLMaster ver. 5; Carl Zeiss Meditec, Dublin, CA, USA), disc photography along with red-free fundus photography (TRC-NW8; Topcon, Tokyo, Japan), standard automated perimetry (Humphrey Field Analyzer II 750, 24-2 Swedish Interactive Algorithm; Carl Zeiss Meditec), as well as spectral domain OCT and OCTA (Spectralis OCT; Heidelberg Engineering, Heidelberg, Germany).

Glaucomatous optic nerve damage was defined as rim thinning, notching, and/or the presence of RNFL defects, and was evaluated by two glaucoma specialists (KML and SHK). POAG was defined as glaucomatous optic nerve damage and associated visual field defects with an open iridocorneal angle (in the case of cataract surgery, the angle was confirmed preoperatively). Glaucomatous visual field defect was defined as (1) outside normal limits on glaucoma hemifield test, (2) three abnormal points, with a *p*-value less than 5% probability of being normal and one with a *p*-value less than 1% by pattern deviation, or (3) pattern standard deviation of less than 5%. Visual field defects were confirmed on two consecutive reliable tests (fixation loss rate of 20%, and false-positive and false-negative error rates of ≤25%). The control group was enrolled from subjects who had been referred as glaucoma suspect but had an intraocular pressure of ≤21 mmHg, a normal optic disc appearance, an open iridocorneal angle, normal red-free fundus photography, and a normal visual field.

The inclusion criteria were POAG patients and control patients. The exclusion criteria were best-corrected visual acuity <20 / 40, a history of ocular surgery other than cataract extraction or corneal refractive surgery, retinal or neurologic disease other than glaucoma that could cause visual field defect, and poor-quality OCTA imaging (quality score, <25). When both eyes were eligible, one eye was randomly selected for the analysis.

Optical coherence tomography angiography

The optic nerve and peripapillary area were imaged us-

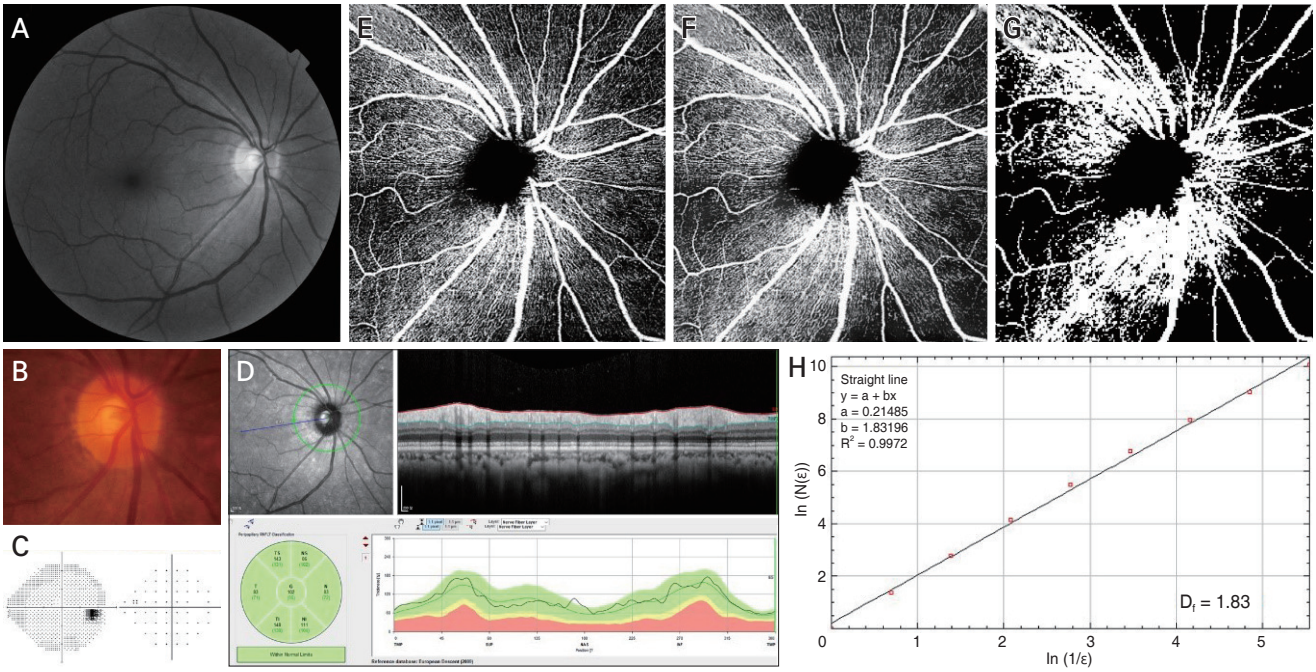

Fig. 1. Fractal dimension calculation. (A) Red-free fundus photography, (B) disc photography, (C) visual field, and (D) optical coherence tomography (OCT) results showing no glaucomatous damage. (D) Average peripapillary retinal nerve fiber layer thickness was 102 μm by OCT. (E) Peripapillary OCT angiography image obtained by predefined *en face* slab of superficial vascular complex (SVC). (F) After applying the nonlocal means denoising filter to reduce background noise, (G,H) the fractal dimension (D_f) was calculated from the converted gray-scale image using the box-counting method provided by the ImageJ software program. (H) The slope of a log–log plot is the fractal dimension of the peripapillary SVC vasculature. In the box-counting method, a grid is drawn and then the number of boxes (N) of the grid that are covering parts of the image is counted. As the grid becomes finer, magnification factor ε increases, and N increases reciprocally. In the pattern with self-similarity-like vessels, the slope of their changes converges: the fractal dimension ($D_f = \log N / \log \varepsilon$), which is calculated as the slope of a log–log plot.

Table 1. Demographic data according to diagnosis

Variable	Primary open-angle glaucoma (n = 64)	Control (n = 33)	*p*-value
Age (yr)	57.2 ± 12.7	57.1 ± 14.0	0.969*
Sex			0.562†
Male	35	16	
Female	29	17	
Refractive error (D)	–3.04 ± 3.49	–2.26 ± 3.64	0.309*
Axial length (mm)	25.00 ± 1.57	24.95 ± 1.66	0.874*
Intraocular pressure (mmHg)	16.10 ± 3.30	13.90 ± 2.10	0.001*
Bruch's membrane opening area (mm^2)	2.56 ± 0.90	2.39 ± 0.61	0.343*
Average RNFL thickness (μm)	75.70 ± 14.10	96.20 ± 9.30	<0.001*
Mean deviation (dB)	–7.54 ± 5.32	–1.07 ± 1.25	<0.001*
Pattern standard deviation (dB)	8.14 ± 4.64	1.96 ± 0.68	<0.001*
Superficial vascular plexus (D_f)	1.74 ± 0.08	1.81 ± 0.05	<0.001*
Avascular complex (D_f)	1.67 ± 0.07	1.68 ± 0.07	0.563*

Values are presented as mean ± standard deviation or number only.
POAG =; D = diopter; RNFL = retinal nerve fiber layer; D_f = fractal dimension.
*Comparison performed using independent *t*-test; †Comparison performed using chi-square test.

ing a commercially available OCTA device (Spectralis OCT) with a central wavelength of 880 nm, an acquisition speed of 85 kHz, and lateral and axial resolutions of 5.7 and 3.9 μm/pixel, respectively. Spectralis OCTA uses a full-spectrum probabilistic approach that computes the probability that a given pixel follows the OCT signal distribution of the perfused vasculature rather than that of static tissue, which affords an almost binary high-contrast image appearance [22]. Scans were obtained from a 20° × 20°-pattern consisting of 512 clusters of five repeated B-scans centered on the optic disc.

To evaluate vascular plexuses, we used predefined slabs of Spectralis OCTA: the superficial vascular complex (SVC; between the inner limiting membrane and constant offsets from the inner plexiform layer) and the avascular complex (AVC; between the outer plexus layer and the Bruch's membrane opening [BMO]) [22]. *En face* images of the predefined Spectralis OCTA slabs were used for the analysis.

Fractal dimension calculation

Images were processed using ImageJ software (National Institutes of Health, Bethesda, MD, USA) (Fig. 1A-1H). First, a nonlocal means denoising filter was applied to reduce the background noise (Fig. 1G). Second, gray-scale

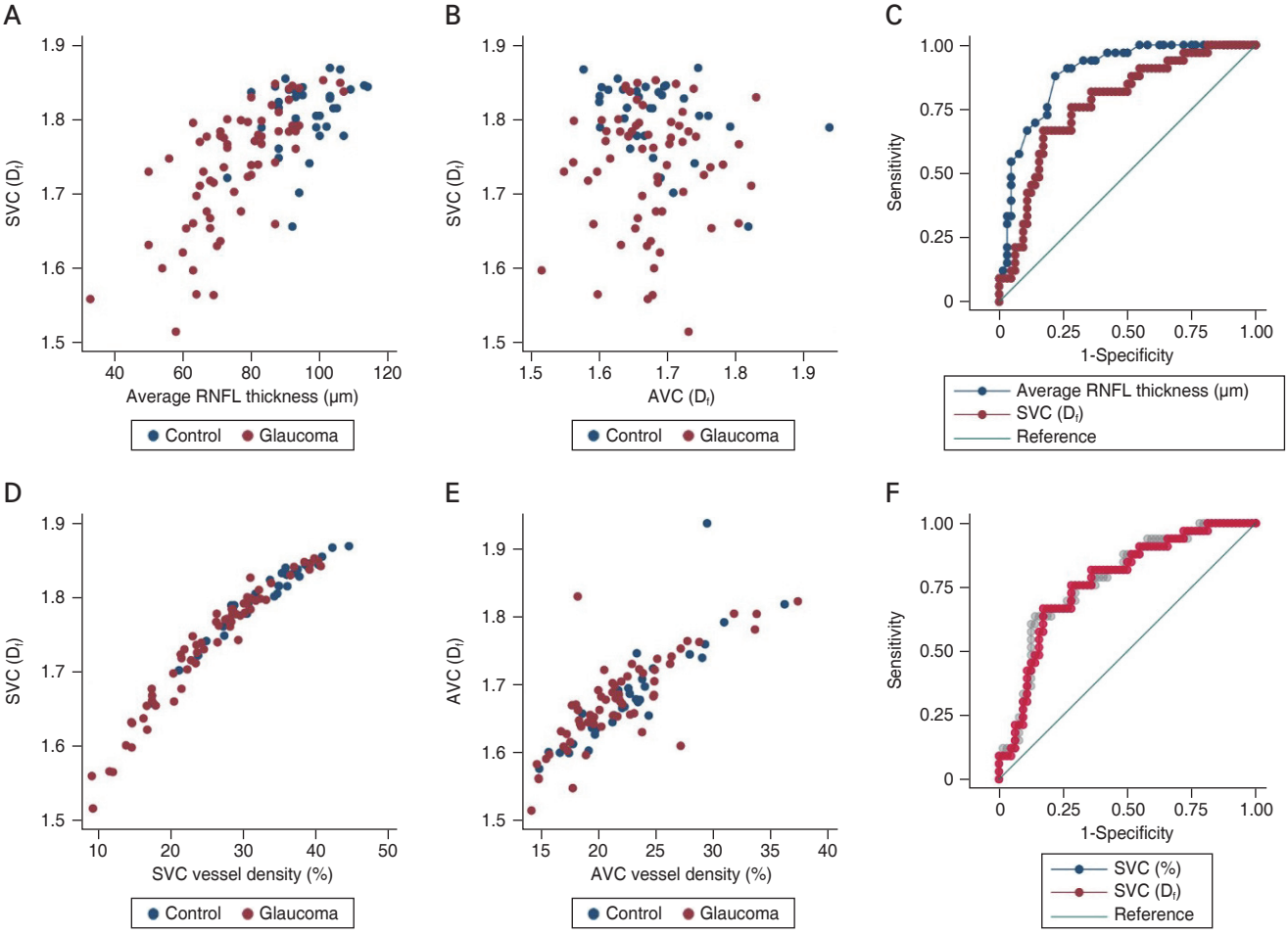

Fig. 2. Scatter plots and receiver operating characteristic (ROC) curves comparing the fractal dimension (D_f) of vascular complex, vessel density, and average retinal nerve fiber layer (RNFL) thickness. (A) The fractal dimension of superficial vascular complex (SVC) and average RNFL thickness show clear correlation (r = 0.723, $p < 0.001$). (B) The fractal dimension of SVC and that of avascular complex (AVC) do not show any correlation (r = –0.010, $p = 0.922$). (C) Area under the ROC curve (AUC) is larger in average RNFL thickness than in the fractal dimension of SVC ($p = 0.008$). (D) The fractal dimension of SVC showed a clear correlation with vessel density of SVC (r = 0.969, $p < 0.001$). (E) The fractal dimension of AVC showed a clear correlation with vessel density of AVC (r = 0.778, $p < 0.001$). (F) The AUC comparison showed no difference between fractal dimension and vessel density of SVC ($p = 0.557$).

images were evaluated for the fractal dimension using the box-counting method provided by the Multifrac plugin of ImageJ software (Fig. 1H) [23]. Box counting relies on the equation $N \propto \varepsilon^{D_f}$, where N is the number of objects, ε is the linear scaling or magnification factor, and D_f is the fractal dimension, which is equivalent to the inverse of the box's linear dimension (Supplementary Fig. 1A-1C). The fractal dimension can be calculated by a log–log plot of N and ε as follows: $D_f = \log N / \log \varepsilon$ (Fig. 1H) [24].

Vessel density calculation

Vessel density was calculated from the same images using ImageJ software. After the images were binarized through Otsu's method, the percentage of vessel-occupied area was calculated [25,26].

Data analysis

The group comparisons were performed by way of the independent *t*-test for the continuous variables and by chi-square testing for the categorical variables. The diagnostic utilities of parameters were determined by calculating the areas under the receiver operating characteristic (ROC) curves (AUCs). The ROC curve shows the trade-off between sensitivity and specificity. An AUC of 1.0 represents perfect discrimination, whereas an AUC of 0.5 represents chance discrimination. The following established five-category rating scale was used for interpretation of AUC values: >0.90, excellent; 0.80–0.90, good; 0.70–0.80, fair; 0.60–0.70, poor; and 0.50–0.60, fail [27]. Univariable and multivariable analyses were run to determine the factors associated with fractal dimension, and parameters with a *p*-value less than 0.10 in the univariable analysis were included from the subsequent multivariable analysis. Statistical analyses were performed with commercially available software (Stata ver. 16.0; Stata Corp., College Station, TX, USA). The data herein are presented as mean ± standard deviations except where stated otherwise, and the cutoff for statistical significance was set to $p < 0.05$.

Results

A total of 113 eyes from 113 participants were recruited between January 2019 and December 2020. Of these, 16

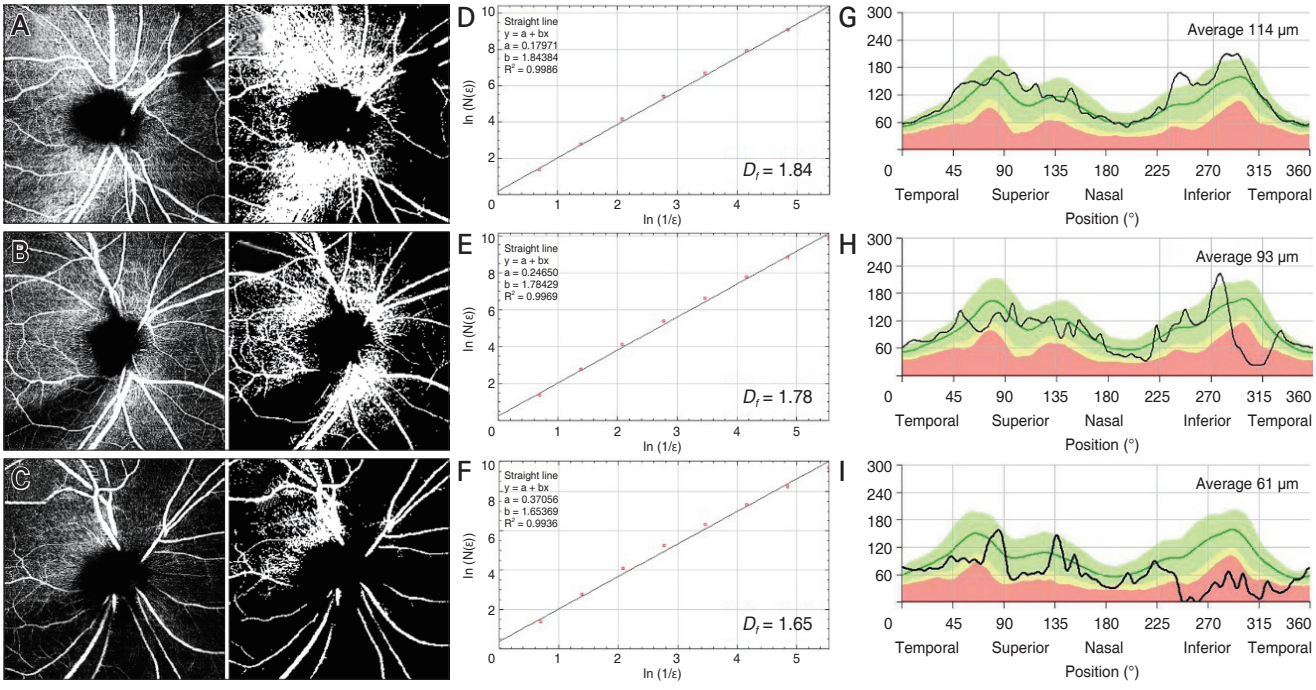

Fig. 3. Representative cases. (A-C) Raw and converted optical coherence tomography angiography images obtained by predefined slab of superficial vascular complex. (D-F) Fractal dimensions (D_f). (G-I) Peripapillary retinal nerve fiber layer (RNFL) thickness maps. Each row contains information on the same subject. As the glaucoma severity increases, the fractal dimension declines, so does the average RNFL thickness.

subjects were excluded due to either poor OCTA image quality or fractal dimension calculation failure, which resulted in a final sample of 97 eyes from 97 subjects (64 POAG eyes and 33 control eyes). Their demographic and clinical characteristics are summarized in Table 1.

The fractal dimension of SVC correlated with the average RNFL thickness (r = 0.723, $p < 0.001$) (Fig. 2A), whereas it did not correlate with that of AVC (r = –0.010, $p = 0.922$) (Fig. 2B). In POAG eyes, the fractal dimension of SVC decreased as the average RNFL thickness decreased according to disease severity (Fig. 3A-3I). The glaucoma-diagnostic utility was excellent for the average RNFL thickness (AUC, 0.889; 95% confidence interval [CI], 0.825–0.953), and good for the fractal dimension of the SVC (AUC, 0.772; 95% CI, 0.675–0.870). The AUC difference was statistically significant ($p = 0.008$) (Fig. 2C).

The fractal dimension showed a good correlation with the vessel density in both SVC (r = 0.969, $p < 0.001$) (Fig. 2D) and AVC (r = 0.817, $p < 0.001$) (Fig. 2E). The glaucoma-diagnostic utility of SVC vessel density (AUC, 0.778; 95% CI, 0.683–0.874) was not statistically different from that of the SVC fractal dimension ($p = 0.557$) (Fig. 2F).

Multivariable regression analyses were performed to reveal the associative factors for each fractal dimension. The fractal dimension of the SVC was higher in subjects of younger age ($p < 0.001$) and with shorter axial length ($p < 0.001$) and thicker average RNFL thickness ($p < 0.001$) (Table 2). The fractal dimension of the AVC, meanwhile, was higher in subjects with larger BMO area ($p = 0.013$, Table 3).

Table 2. Factors associated with fractal dimension of superficial vascular complex

Factor	Univariable analysis			Multivariable analysis*		
	Coefficient	95% CI	*p*-value	Coefficient	95% CI	*p*-value
Age (yr)†	–0.002	–0.003 to –0.001	0.003	–0.002	–0.003 to –0.001	<0.001
Female sex (vs. male sex)	0.038	0.007 to 0.069	0.017	–0.014	–0.038 to 0.010	0.252
Axial length (mm)†	–0.010	–0.020 to 0.000	0.057	–0.018	–0.027 to –0.009	<0.001
Intraocular pressure (mmHg)	–0.006	–0.011 to –0.001	0.029	–0.001	–0.005 to 0.002	0.477
Bruch's membrane opening area (mm^2)	–0.008	–0.028 to 0.011	0.401	-	-	-
Average RNFL thickness (μm)†	0.004	0.003 to 0.004	<0.001	0.003	0.002 to 0.004	<0.001
Glaucoma diagnosis (vs. control)	–0.069	–0.100 to –0.038	<0.001	–0.004	–0.032 to 0.024	0.773
Avascular complex (D_f)	–0.038	–0.276 to 0.200	0.753	-	-	-

CI = confidence interval; RNFL = retinal nerve fiber layer; D_f = fractal dimension.
*Variables with $p < 0.10$ in the univariable analysis were included in the subsequent multivariable analysis; †Statistically significant ($p < 0.05$).

Table 3. Factors associated with fractal dimension of avascular complex

Factor	Univariable analysis			Multivariable analysis*		
	Coefficient	95% CI	*p*-value	Coefficient	95% CI	*p*-value
Age (yr)	–0.000	–0.002 to 0.001	0.349	-	-	-
Female sex (vs. male sex)	–0.033	–0.060 to –0.006	0.016	–0.025	–0.053 to 0.003	0.082
Axial length (mm)	0.008	–0.000 to 0.027	0.058	–0.001	–0.011 to 0.009	0.812
Intraocular pressure (mmHg)	–0.001	–0.006 to 0.003	0.550	-	-	-
Bruch's membrane opening area (mm^2)†	0.027	0.010 to 0.043	0.002	0.024	0.005 to 0.043	0.013
Average RNFL thickness (μm)	–0.000	–0.001 to 0.001	0.922	-	-	-
Glaucoma diagnosis (vs. control)	–0.008	–0.037 to 0.021	0.563	-	-	-
Superficial vascular complex (D_f)	–0.028	–0.202 to 0.147	0.753	-	-	-

CI = confidence interval; RNFL = retinal nerve fiber layer; D_f = fractal dimension.
*Variables with $p < 0.10$ in the univariable analysis were included in the subsequent multivariable analysis; †Statistically significant ($p < 0.05$).

Discussion

In this study, we compared the vascular complexities between POAG and control subjects using fractal dimension analysis. The fractal dimension was smaller in the superficial layer, while it showed no difference in the deeper layer of POAG patients when assessed with OCTA images. Moreover, the fractal dimension of the superficial layers showed a significant correlation with the average RNFL thicknesses. This implied that the fractal dimension of the superficial retinal vasculature can be used as a marker reflecting glaucoma severity quantitatively.

The fractal dimension is a ratio providing a statistical index of complexity, which describes the space-filling capacity of a pattern by the noninteger dimension: a lacunar structure has a dimension value of between 1 (line) and 2 (plane). To define the fractal dimension, we used the box-counting method. In this method, a grid is drawn to the given pattern and then the number of boxes of the grid that are covering parts of the image is counted. As the grid becomes finer, magnification factor ε increases, and the number of boxes (N) increases reciprocally. In the pattern with self-similarity-like vessels, the slope of their changes converges to the fractal dimension. As arborizing structures, the vessels are very suitable for evaluation of the fractal dimension. In contrast to density, the fractal dimension is unaffected by the size of the surface plane, and thus it has the potential for more robust parameters of vascularity. The fractal dimension has been used for evaluation of macular vascularity in diabetic retinopathy [12], hypertensive retinopathy [17], and age-related macular degeneration [16]. In POAG, the fractal dimension has been used for evaluation of ONH vascularity as measured by Heidelberg Doppler flowmetry [18]. To the best of our knowledge, however, fractal dimension analysis was not used to evaluate the layer-by-layer vascularity of the ONH and peripapillary area, which has been possible only since the recent advent of OCTA.

Among the fractal dimensions of the ONH layers, that of the SVC showed a close correlation with the average RNFL thickness. Since the vessels in the superficial layer supply the RNFL layer, RNFL thickness might be closely associated with superficial vascularity as assessed by the fractal dimension. In healthy subjects, the peripapillary retinal vasculature showed a significant correlation with peripapillary retinal thickness when assessed with OCTA [28]. Lee et al. [29] demonstrated the topographic relationship between decreased superficial parapapillary vascularity and localized RNFL defects. In the present study, we derived a new quantitative means of describing vascularity. Furthermore, RNFL thickness shows large variations among individuals and OCT machines, whereas the fractal dimension is a standardized parameter between 1 and 2. Therefore, the fractal dimension of superficial retinal vascularity may have potential as a new ONH parameter for assessment of glaucoma.

The fractal dimension of the AVC, however, did not show any correlation with RNFL thickness in our study. Since the deep vessels in the ONH rarely supply the retinal layers, they would not be affected by RNFL thickness. In our study, the fractal dimension of AVC was associated with BMO area. A larger BMO would enable better visualization of underlying vessels, resulting in a higher fractal dimension.

In this study, we introduced a new parameter, fractal dimension of vascular complex, for ONH-evaluation purposes. Although the fractal dimension of the SVC was not superior to the average RNFL thickness in glaucoma diagnosis, the concept of assessing vascularity would be very helpful, since this analysis provides us with a quantitative value for further analysis. Although the fractal dimension of the vasculature showed a clear correlation with the vessel density and their glaucoma-diagnostic abilities were similar, we considered that the fractal dimension has a theoretical strength for the purposes of a future study, since it is less affected by the limitation imposed by the resolution (Supplementary Fig. 1D-1F). The average RNFL thickness did not match exactly with the fractal dimension of the SVC, the discrepancy between them might be useful for ONH categorization according to etiology. Moreover, the fractal dimensions of other layers might be useful in future evaluations of vascular pathology in the deep ONH structure.

This study has several limitations. First, all of the participants were South Korean, and there may be ethnic differences in ONH morphology [30]. Second, about 14% of the enrolled subjects were excluded due to poor image quality or fractal dimension calculation failure. Calculation algorithms should be improved for more general use. Third, it is known that different OCTA machines provide different vascular indices [21]; therefore, our results may not be directly translatable into other OCTA machines. We specu-

late, however, that the concept of fractal dimension analysis could be incorporated into any OCTA machines other than Spectralis OCT. Fourth, the control group was enrolled from glaucoma-suspect patients, and diagnostic utility depends on a study population: there will be higher diagnostic utility in the severe-glaucoma patients/healthy control subjects setting, while there will be lower diagnostic utility in the early-glaucoma patients/glaucoma-suspect patients setting. Therefore, the diagnostic utility observed in this study should be interpreted cautiously in the contexts of other populations. Fifth and finally, the fractal dimension of vascular complex does not measure the vascular flow the same as it does the vascular density. If ONH perfusion status could be reliably imaged in the future though, the fractal dimension of perfusion status would provide meaningful serial quantitative parameters for assessment of glaucoma patients.

In conclusion, the layered ONH vascularity could be analyzed quantitatively by adopting fractal dimension analysis of OCTA images. The fractal dimension of the SVC correlated with the average RNFL thickness, and it was reduced in POAG patients. The fractal dimension of vascular complex could be a novel standardized marker for assessment of vascularity in glaucoma of various etiologies.

Conflicts of Interest: None.
Acknowledgements: None.
Funding: This research was supported by a grant of the Korea Health Technology R&D Project through the Korea Health Industry Development Institute (KHIDI), funded by the Korean government (the Ministry of Health and Welfare) (No. HI22C1234). The funders had no role in the study design, data collection and analysis, decision to publish, or preparation of the manuscript.

Supplementary Materials

Supplementary Fig. 1. Fractal dimension analysis.
Supplementary materials are available at https://doi.org/10.334/kjo.2022.0089.

References

1. Chung HS, Harris A, Kagemann L, Martin B. Peripapillary retinal blood flow in normal tension glaucoma. *Br J Ophthalmol* 1999;83:466-9.
2. Sehi M, Goharian I, Konduru R, et al. Retinal blood flow in glaucomatous eyes with single-hemifield damage. *Ophthalmology* 2014;121:750-8.
3. Tielsch JM, Katz J, Sommer A, et al. Hypertension, perfusion pressure, and primary open-angle glaucoma: a population-based assessment. *Arch Ophthalmol* 1995;113:216-21.
4. Bonomi L, Marchini G, Marraffa M, et al. Vascular risk factors for primary open angle glaucoma: the Egna-Neumarkt Study. *Ophthalmology* 2000;107:1287-93.
5. Leske MC, Connell AM, Wu SY, et al. Risk factors for open-angle glaucoma: the Barbados Eye Study. *Arch Ophthalmol* 1995;113:918-24.
6. Quigley HA, Hohman RM, Addicks EM, Green WR. Blood vessels of the glaucomatous optic disc in experimental primate and human eyes. *Invest Ophthalmol Vis Sci* 1984;25:918-31.
7. Cull G, Burgoyne CF, Fortune B, Wang L. Longitudinal hemodynamic changes within the optic nerve head in experimental glaucoma. *Invest Ophthalmol Vis Sci* 2013;54:4271-7.
8. Liu L, Jia Y, Takusagawa HL, et al. Optical coherence tomography angiography of the peripapillary retina in glaucoma. *JAMA Ophthalmol* 2015;133:1045-52.
9. Yarmohammadi A, Zangwill LM, Diniz-Filho A, et al. Optical coherence tomography angiography vessel density in healthy, glaucoma suspect, and glaucoma eyes. *Invest Ophthalmol Vis Sci* 2016;57:OCT451-9.
10. Chen CL, Zhang A, Bojikian KD, et al. Peripapillary retinal nerve fiber layer vascular microcirculation in glaucoma using optical coherence tomography-based microangiography. *Invest Ophthalmol Vis Sci* 2016;57:OCT475-85.
11. Akagi T, Iida Y, Nakanishi H, et al. Microvascular density in glaucomatous eyes with hemifield visual field defects: an optical coherence tomography angiography study. *Am J Ophthalmol* 2016;168:237-49.
12. Daxer A. The fractal geometry of proliferative diabetic retinopathy: implications for the diagnosis and the process of retinal vasculogenesis. *Curr Eye Res* 1993;12:1103-9.
13. Landini G, Misson GP, Murray PI. Fractal analysis of the normal human retinal fluorescein angiogram. *Curr Eye Res* 1993;12:23-7.

14. Avakian A, Kalina RE, Sage EH, et al. Fractal analysis of region-based vascular change in the normal and non-proliferative diabetic retina. *Curr Eye Res* 2002;24:274-80.
15. Masters BR. Fractal analysis of the vascular tree in the human retina. *Annu Rev Biomed Eng* 2004;6:427-52.
16. Cheung E, Jiminez A, Busuioc M, Smith RT. Fractal analysis of age related macular degeneration. *Invest Ophthalmol Vis Sci* 2009;50:312.
17. Kurniawan ED, Cheung N, Cheung CY, et al. Elevated blood pressure is associated with rarefaction of the retinal vasculature in children. *Invest Ophthalmol Vis Sci* 2012;53:470-4.
18. Ciancaglini M, Guerra G, Agnifili L, et al. Fractal dimension as a new tool to analyze optic nerve head vasculature in primary open angle glaucoma. *In Vivo* 2015;29:273-9.
19. Huang F, Dashtbozorg B, Zhang J, et al. Reliability of using retinal vascular fractal dimension as a biomarker in the diabetic retinopathy detection. *J Ophthalmol* 2016;2016:6259047.
20. Orlando JI, van Keer K, Barbosa Breda J, et al. Proliferative diabetic retinopathy characterization based on fractal features: evaluation on a publicly available dataset. *Med phys* 2017;44:6425-34.
21. Corvi F, Pellegrini M, Erba S, et al. Reproducibility of vessel density, fractal dimension, and foveal avascular zone using 7 different optical coherence tomography angiography devices. *Am J Ophthalmol* 2018;186:25-31.
22. Rocholz R, Teussink MM, Dolz-Marco R, et al. SPECTRALIS optical coherence tomography angiography (OCTA): principles and clinical applications. *Heidelb Eng Acad* 2018;Sep:1-10.
23. Torre IG, Heck RJ, Tarquis AM. MULTIFRAC: an ImageJ plugin for multiscale characterization of 2D and 3D stack images. *SoftwareX* 2020;12:100574.
24. Mandelbrot B. *The fractal geometry of nature.* New York: W. H. Freeman & Co; 1982.
25. Al-Sheikh M, Phasukkijwatana N, Dolz-Marco R, et al. Quantitative OCT angiography of the retinal microvasculature and the choriocapillaris in myopic eyes. *Invest Ophthalmol Vis Sci* 2017;58:2063-9.
26. Park SY, Nam KT, Yun C, Jang S. Analyses of vessel densities and foveal avascular zones using four optical coherence tomography angiography devices. *J Korean Ophthalmol Soc* 2020;61:482-90.
27. Swets JA. Measuring the accuracy of diagnostic systems. *Science* 1988;240:1285-93.
28. Yu J, Gu R, Zong Y, et al. Relationship between retinal perfusion and retinal thickness in healthy subjects: an optical coherence tomography angiography study. *Invest Ophthalmol Vis Sci* 2016;57:OCT204-10.
29. Lee EJ, Lee KM, Lee SH, Kim TW. OCT angiography of the peripapillary retina in primary open-angle glaucoma. *Invest Ophthalmol Vis Sci* 2016;57:6265-70.
30. Lim LS, Matsumura S, Htoon HM, et al. MRI of posterior eye shape and its associations with myopia and ethnicity. *Br J Ophthalmol* 2020;104:1239-45.